coatings

Article

Characterization and Wear Behaviors of Electrodeposited Ni-MoS_2/SiC Composite Coating

Yutao Yan [1,*], Lifeng Lu [1], Yuqiu Huo [2,*] and Yong Zhao [1]

[1] School of Mechanical Engineering and Automation, Northeastern University, Shenyang 110819, China
[2] Department of Chemistry, College of Science, Northeastern University, Shenyang 110819, China
* Correspondence: ytyan@mail.neu.edu.cn (Y.Y.); huoyuqiu@mail.neu.edu.cn (Y.H.)

Abstract: Among the preparation methods of functional coatings, the electrodeposition technique has attracted much attention due to its advantages of economy, high efficiency and good structural adaptability. The application of aluminum alloy materials is greatly limited due to their poor friction reduction and wear resistance. Therefore, to enhance the tribological behaviors of aluminum alloy materials, the Ni-MoS_2, Ni-SiC and Ni-MoS_2/SiC composite coatings were prepared on the 2218 aluminum alloy by an electrodeposition technique. The prepared composite coating samples exhibited a compact and dense microstructure, which was consistent with the result of their high microhardness. No obvious microcracks and defects appeared at the interfaces, indicating that the composite coating samples had good adhesion to the substrates and can effectively improve the frictional shear resistance. The results of wear experiment showed that the wear rate, friction coefficient and friction response time of all composite coating samples were lower than that of the substrate sample. However, the friction reduction and wear resistance of the same composite coating sample were not consistent. The friction coefficient of the Ni-MoS_2 composite coating sample was the lowest, and the wear rate of the Ni-SiC composite coating sample was the lowest. According to the worn surface observations, the wear mechanism of composite coating samples was mainly characterized by the mild abrasive wear, flake spalling, tearing and pits caused by particle shedding, and the substrate sample showed a severe adhesive wear and abrasive wear.

Keywords: electrodeposition; composite coating; microstructure; friction; wear mechanism

Citation: Yan, Y.; Lu, L.; Huo, Y.; Zhao, Y. Characterization and Wear Behaviors of Electrodeposited Ni-MoS_2/SiC Composite Coating. *Coatings* **2022**, *12*, 1223. https://doi.org/10.3390/coatings12081223

Academic Editor: Alexander D. Modestov

Received: 4 August 2022
Accepted: 18 August 2022
Published: 21 August 2022

1. Introduction

Two contacting elements with relative sliding in industrial equipment may reduce the service life and cause more economy and energy losses due to surface wear, and even lead to their failure [1,2]. The research of surface coating technique, which reduces wear and improves service life and reliability of industrial equipment by preparing a protective coating on the contact surface, has aroused great interest [3–5]. Laser cladding [6], chemical/physical vapor deposition [7,8], plasma spraying [9] and electrodeposition [10] are all commonly used as surface coating techniques to enhance wear resistance of materials. Among these methods, the electrodeposition method has received much attention owing to its low cost, ease of implementation and applicability to various geometries [11–15].

In order to obtain a coating with excellent tribological properties, the commonly used surface coating materials are hard ceramic particles such as SiC, WC, Al_2O_3, and excellent solid lubricants such as MoS_2, graphite, GO and so on [3,16–19]. The improved wear resistance of coatings containing SiC particles is attributed to an increase in the hardness [3,20]. The increase of SiC particle content in the electrodeposited Ni-SiC composite coating can effectively improve its hardness, and reduce the wear rate and friction coefficient. The wear mechanism of the coatings mainly includes abrasive wear and oxidation wear under dry wear test [16,21]. Sun et al. [22] successfully prepared the Ni-SiC coating on mild steel by a magnetically assisted pulse electrodeposition method. The results showed that the Ni-SiC coating had higher hardness and good wear resistance. Yazdani and Zakeri [23] obtained the Ni-SiC composite nanocomposite coating on aluminum-based materials by a high energy ball milling technique. It can be found that the microstructure, mechanical performances and wear resistance obviously depended on the charge composition, and the dispersion strengthening effect of composite materials could reduce the grain size of SiC particles and Ni matrix to the nanoscale. Ji et al. [24] proposed a method for the preparation of Ni-SiC coating by rotating magnetic-field-assisted electrodeposition. The results showed that the surface morphology was effectively improved and the defects were reduced because the rotating magnetic field reduced the agglomeration of SiC particles. The thickness, hardness and adhesion of the coating were then significantly improved. In addition, the tribological behaviors of composite coatings of SiC with MoS_2 [25], PTFE [26], graphite [27], BN [28] or GO [29] were also widely investigated. The results showed that the friction reduction and wear resistance of the composite coating containing hard particles and self-lubricating powder were significantly improved compared to the substrate materials. Likewise, MoS_2 solid lubricants with excellent lubrication properties are also often selected as coating materials in the research of coating technique. Maharana et al. [30] successfully prepared the Ni-MoS_2 coating by means of the electrodeposition method, and investigated its mechanical and tribological performances. It can be found that the wear resistance of coatings depends primarily on a combined effect of coating morphology and hardness caused by dispersion hardening and crystal orientation. He et al. [31] studied the tribological behaviors of the Ni-P-MoS_2 composite coating deposited on mild steel. It is interesting that the composite coating had a very small wear rate and friction coefficient. The MoS_2 particles had been broken into slender fragments, which may be one of the reasons for their excellent tribological properties. Furthermore, the MoS_2 content in the plating solution had a significant effect on the surface roughness of the coating. Under current-carrying tribological conditions, the low friction coefficient of MoS_2-based coatings was mainly due to the high adhesion and a higher density transfer film of the coating materials on the metal surface, meanwhile the high wear rate was determined by the high roughness surface caused by the heat release from the current and enhanced abrasive properties [32]. The reorientation and compaction of porous MoS_2 coating materials can be achieved by friction pretreatment, which effectively inhibits the formation of wear debris. As a result, the MoS_2 coating had good friction reduction and wear resistance [33–36]. Multi-phase composite coatings containing MoS_2 particles and diamond-like carbon [37], Si_3N_4 [38] or CeO_2 [39] were prepared, their tribological properties were investigated and the wear mechanism was explored. As a result, the addition of MoS_2 had effectively enhanced the friction reduction and wear resistance of the metal materials.

The motivation of this work is to obtain a composite coating with good tribological behaviors on aluminum alloy substrates to enhance their wear resistance. To achieve this purpose, the hard SiC ceramic particles and solid MoS_2 lubricant were selected as coating materials, and the Ni-SiC, Ni-MoS_2 and Ni-MoS_2/SiC composite coatings were prepared on the surface of 2218 aluminum alloy by an electrodeposition method. The surface morphologies, microstructure, microhardness and interfacial bonding strength were investigated. The tribological behaviors were discussed under dry sliding friction, and the wear mechanism was explored.

2. Experimental Procedures

2.1. Materials and Chemicals

Molybdenum disulfide (MoS_2) and silicon carbide (SiC) were commercially purchased from Shanghai Chaowei Nanotech Co., Ltd., Shanghai, China. The 2218 aluminum alloy chosen as the substrate material was purchased from Dongguan Avis Metal Materials Co., Ltd., Dongguan, China. The chemicals used were commercially purchased. The information of all materials is shown in Tables 1–3.

Table 1. The coating materials and properties.

Materials	Average Particle Size (nm)	Specific Surface Area ($m^2 \cdot g^{-1}$)	Density ($g \cdot cm^{-3}$)	Purity (%)
MoS_2	600	12.4	1.83	≥99.9
SiC	600	3.2	1.52	≥99.5

Table 2. Chemical composition of 2218 aluminum alloy substrate.

Elements	Fe	Si	Mn	Cu	Mg	Al
wt.%	0.5	0.35	0.28	1.8	2.6	balanced

Table 3. The chemicals.

Chemicals	Purity (%)	Brand
$Ni(NH_2SO_3)_2 \cdot 4H_2O$	99	Macklin
$CH_3(CH_2)_{11}OSO_3Na$	98	Aiyan
HBO_3	99.5	Nanshi
Na_2CO_3	99.8	Nanshi
Na_3PO_4	98	Nanshi
NaOH	96	Nanshi
HNO_3	65–68	Aladdin
ZnO	99	Aiyan
$FeCl_3$	97	Nanshi
$C_6H_8O_7$	99.5	Macklin
$NaNO_3$	99	Nanshi

2.2. Deposition of the Composite Coatings

The surface of the 2218 aluminum alloy disc samples (ϕ 50 mm × 8 mm) was polished using 400, 600, 800 and 1000 grain metallographic sandpapers in a certain order [10,40]. The surface roughness was measured to be ~0.22 µm with a TR 200 surface roughness meter with an accuracy of 0.001 µm (Beijing Saiboruixin technology Co., Ltd., Beijing, China). The electrodeposition device consists of a WYK-5010 DC-regulated voltage and current power supply with an output voltage of 0–50 V and output current of 0–10 A (Yangzhou Jintong Eletronics Co., Ltd., Yangzhou, China) and a DF-101S collector type thermostatic heating magnetic stirrer with a rotation speed of 0–2600 rpm and a temperature of ~400 °C (Gongyi Yuhua Instrument Co., Ltd., Zhengzhou, China). The stable current density is provided by a power supply, and the constant plating solution temperature and continuous stirring are ensured by the thermostatic heating magnetic stirrer. Furthermore, the pretreated aluminum alloy disc was taken as a cathode, and a nickel plate (60 mm × 60 mm × 2 mm) was used as the anode. A distance of 30 mm was maintained between the nickel plate and the aluminum alloy disc. Table 4 shows the operating conditions of electrodeposition determined based on the literature [10,11,16,21,25] and pre-experiments.

Table 4. The operating conditions.

Parameters	Quantity
pH	3.5
Stirring speed n (rpm)	350
Plating solution temperature T (°C)	50
Current density J ($A \cdot dm^{-2}$)	4
Deposition time t (min)	60

The specific process of preparing composite coating is as follows:

Step 1—The aluminum alloy disc samples were etched to remove contaminants and surface oxides in an alkali mixed solution for 2 min.

Step 2—The aluminum alloy disc samples were washed in an acid solution for 30 s.

Step 3—The aluminum alloy disc samples were treated with zinc immersion in the mixed solution for 60 s. Afterwards, the zinc was dezincified in HNO_3 solution for 30 s. Finally, the second zinc immersion was carried out in the mixed solution for 40 s.

Step 4—According to the operating conditions in Table 4 and composite coating requirements, the pretreated aluminum alloy disc samples were subjected to composite coating electrodeposition in plating solution for 60 min.

After each step, the treated aluminum alloy disc samples were ultrasonically cleaned by deionized water for 5 min. Thus, the Ni-MoS_2, Ni-SiC and Ni-MoS_2/SiC composite coatings were achieved. For the convenience of subsequent analysis, the samples of aluminum alloy substrate, Ni-MoS_2 coating, Ni-SiC coating and Ni-MoS_2/SiC coating are denoted as E0, E1, E2 and E3, respectively. The solution composition, operating time and technological process is illustrated in Figure 1.

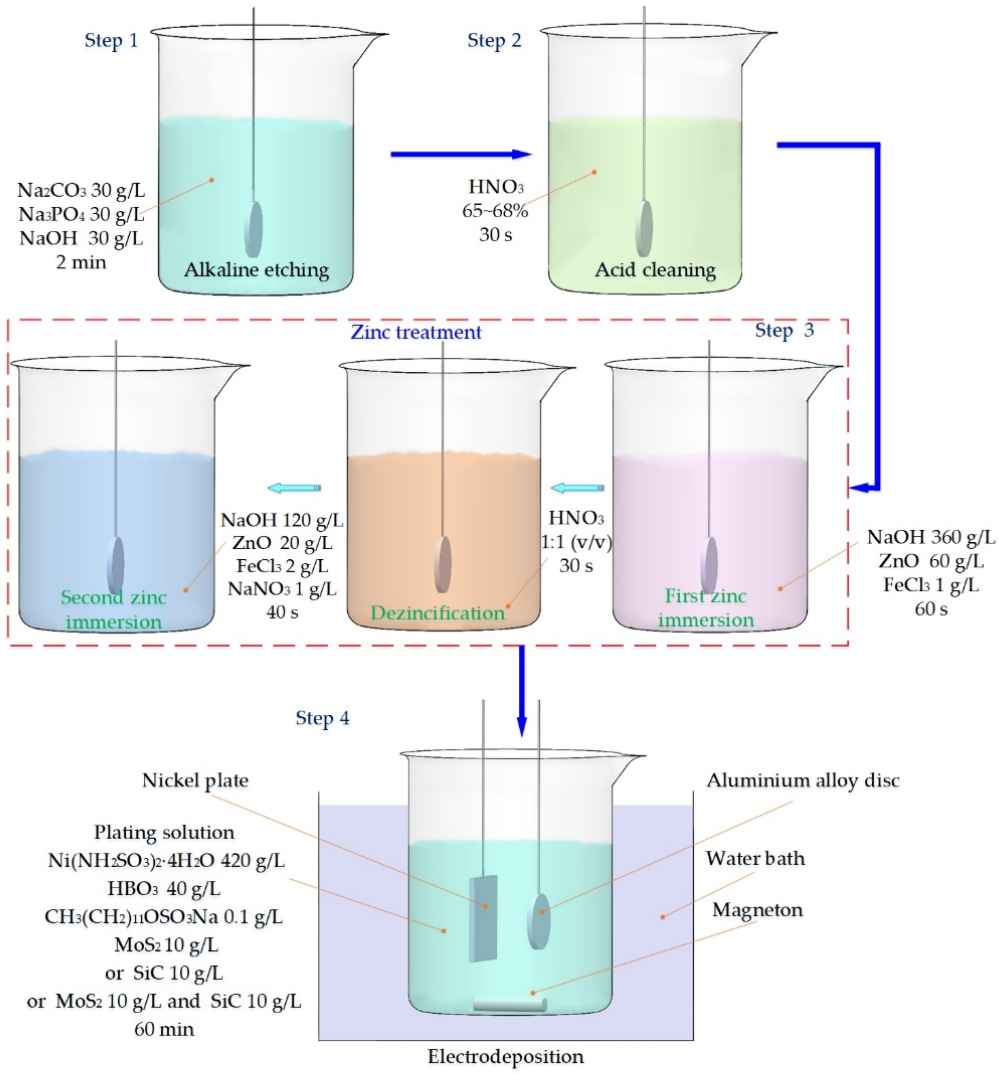

Figure 1. Flow diagram of the technological process.

2.3. Wear Experiments

To investigate the tribological behaviors, the experiments were carried out on a ball-on-disc type tester (HT-1000, Zhongke Kaihua Technology Development Co., Ltd., Lanzhou, China) against the AISI 52100 steel balls with a diameter of 5 mm and micro-hardness of 780 HV. The tester with a load of 1.5–20 N, a rotation speed of 5–2800 rpm and a temperature of room temperature—1000 °C and schematic diagram are shown in

Figure 2. The friction coefficient was automatically obtained during the experiment by the tester. The dry wear experiments were performed at a rotation speed of 400 rpm, a radius of 6 mm, a load of 2 N, a temperature of 100 °C and a time of 10 min based on the purpose of the experiment and pre-experimental analysis. The wear mass loss was obtained by using an electronic balance with an accuracy of 0.1 mg and a weighing capacity of 200 g (FA2204C, Shanghai Yueping Scientific Instrument Co., Ltd., Shanghai, China). The wear rate, W_R, was then calculated by the formula $W_R = \Delta W/PS$, where ΔW is the wear mass loss (mg), P is the normal load (N) and S is the sliding distance (m). Before and after each test, the samples were ultrasonically cleaned using deionized water for 5 min. At least three tests were completed for each condition.

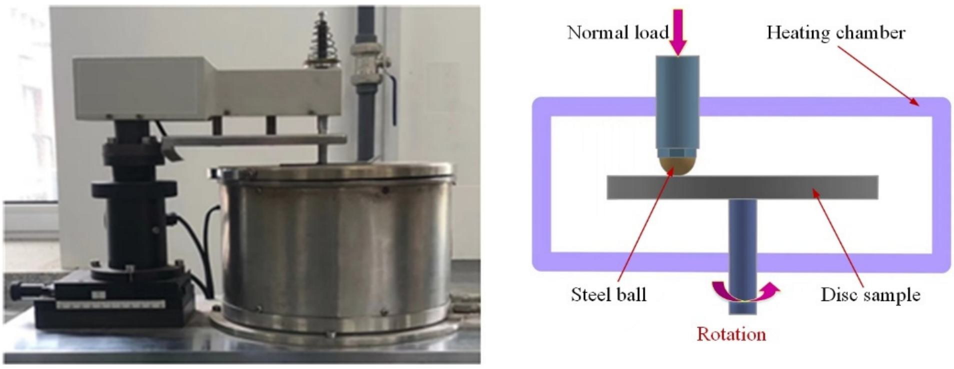

Figure 2. Tester and schematic diagram of ball-on-disc configuration.

2.4. Characterization

Scanning electron microscopy (SEM, MIRA3, TESCAN, Czech Republic) with the energy dispersive spectroscopy (EDS) function was employed to analyze the surface morphologies, cross-section microstructures, worn surface morphologies and element distribution of the samples. In addition, a 3D optical microscope (DVM6, Wetzlar, Germany) was employed to analyze the three-dimensional morphologies and obtain wear depth. A digital Vickers hardness tester (THV-5, Beijing Time High Technology Co., Ltd., Beijing, China) was applied to measure the microhardness of all samples. In this work, the load applied was 200 g and the holding time was 15 s. For the validity of the results, at least 5 points were measured at different locations according to GB/T 4340. The average value was taken as the surface microhardness of the sample. The bonding strength of the composite coatings was obtained using an automatic scratch instrument with a loading rate of 10–100 N/min, a scratch rate of 1–10 mm/min and a scratch length of 2–6 mm (WS-2005, Zhongke Kaihua Technology Development Co., Ltd., Lanzhou, China) according to the method in references [41,42]. In this case, a diamond indenter with a 120° conical shape and a tip radius of 200 µm was employed, and a scratch rate of 6 mm/min and a loading rate of 20 N/min were used. The average value of the results measured at three different locations was used as the bonding strength of the composite coating.

3. Results and Discussion

3.1. Characterization of Composite Coatings

The SEM images and EDS mappings of original surface of all composite coatings are shown in Figure 3. The composite coating of the E1 sample has an irregular and rough morphology with nodules similar to sunflower stamens. However, it can be observed that the distribution of composite coating particles is relatively homogeneous. It is believed that this composite coating structure is because MoS_2 particles attached to the substrate not only become nucleation sites for Ni growth, but also result in higher current density on the surface. Ni ions prefer to nucleate on the particles' surfaces rather than around the particles, resulting in nodular structures. Shourije et al. [43] and He et al. [31] reported the strong influence of conducting particles on the local current distribution and its growth kinetics during the electrodeposition process. In addition, the MoS_2 particles enhance the denseness of the composite coating structure. The presence of MoS_2 particles hinders the growth of Ni ions, resulting in smaller Ni grains, as shown in Figure 3(a1). Similar structural morphology has also been observed by Zhou et al. [44] and He et al. [28]. The EDS mappings in Figure 3(a2) illustrate that uniform Ni, S and Mo elements are enriched on the surface, indicating that the Ni-MoS_2 composite coating was achieved. As shown in Figure 3(b1,b2), compared with the E1 sample, the surface of the E2 sample has a smoother and denser microstructure, and the Ni grains are finer. The SiC particles are irregularly distributed on the surface of the composite coating without any obvious agglomeration. This should be attributed to the fact that the addition of SiC particles increases the number of nucleation sites of Ni crystals while effectively inhibiting the growth of Ni grains [10,45]. Gyawali et al. [46] and Huang et al. [16] described the similar structural morphology of Ni-SiC coating prepared by electrodeposition methods. The EDS mappings indicate that the Ni-SiC composite coating is prepared. As shown in Figure 3(c1), the surface of the E3 sample is a relatively smooth and compact microstructure. The MoS_2 and SiC particles show irregular and relatively uniform distribution, and some SiC particles are wrapped by the layered MoS_2 particles. Compared with the E1 sample, the coronal protrusion of the nodules is finer and the composite coating is more compact, which may be one of the reasons for its higher microhardness. The combined effect of the two coating particles enhances the nucleation sites of Ni ions, and the growth of Ni grains is inhibited. However, the refinement of the Ni grains is inferior to that of the E2 sample, which could be attributed to the addition of MoS_2 particles leading to a change in the current distribution, thus attenuating the inhibitory effect of the SiC particles. Based on the distribution of Ni, Mo, S, Si and C elements in the EDS mappings in Figure 3(c2), it can be concluded that the Ni-MoS_2/SiC composite coating has been successfully obtained.

Figure 4 shows the SEM cross-section images of the composite coating samples. It can be found that the coating thickness of the E2 sample is relatively thin, about 41 μm, which is 71.93% and 89.13% of the E1 and E3 samples. It can be concluded that the thickness of coating mainly depends on the properties of the deposited particle and the electrodeposition rate. The internal structure of all composite coatings is compact, integral and consequent, tightly fitted with the 2218 aluminum alloy substrate. No microcracks and visible pinhole defects were observed at the interface between the composite coatings and the 2218 aluminum alloy substrate, indicating that the electrodeposited composite coatings are well bonded to the 2218 aluminum alloy substrate. However, the surface flatness of the composite coatings is different. The surface of the composite coating of the E2 sample is relatively smoother.

To better illustrate the electrodeposition mechanism of coating particles, the electrodeposition process of the Ni-MoS_2/SiC composite coating is shown in Figure 5. The dispersed SiC and MoS_2 particles in the plating solution are wrapped by Ni ions through weak adsorption, which causes the particles to be transported towards the cathode (aluminum alloy substrate) under electric field forces due to their positive charge. Afterwards, the charged particles pass through the boundary layer and gradually diffuse to the cathode surface. The particles are then adsorbed on the surface of the aluminum alloy substrate to achieve electrodeposition. In the continuous electrodeposition process, the particles in the diffusion layer on the surface near the cathode are continuously reduced. The continuous magnetic stirring effect can cause the charged particles to transfer to the diffusion layer by migration and diffusion, thus ensuring continuous electrodeposition.

3.2. Mechanical Performances

In general, it is believed that the surface hardness and interfacial bonding strength are closely related to their tribological properties. Figure 6 shows the surface microhardness and bonding strength of experimental samples. The hardness is often used to evaluate a material's wear resistance, cutting and scratching properties [10,47–49]. To investigate the effect of surface microhardness on its tribological properties, the microhardness of experimental samples is measured. The surface microhardness of the E0, E1, E2 and E3 samples are illustrated in Figure 6a. The results show that the microhardness of the composite coating samples is significantly enhanced compared to the E0 sample. The trend of increased microhardness of the Ni-MoS_2 and Ni-SiC composite coatings has also been reported in the literature [46,50]. The surface microhardness of the E2 sample is the highest with its value of 407.48 HV, which is consistent with that reported by Huang [16]. The surface microhardness of the E2 sample reaches 3.14 times that of the E0 sample. Likewise, the surface microhardnesses of the E1 and E3 samples are improved by 111.92% and 175.13% compared to the E0 sample, respectively. The increase in surface microhardness is chiefly attributed to the strengthening of the co-deposited particles, the finer structure and the grain refinement due to the hindrance of dislocation migration and grain growth [16,25].

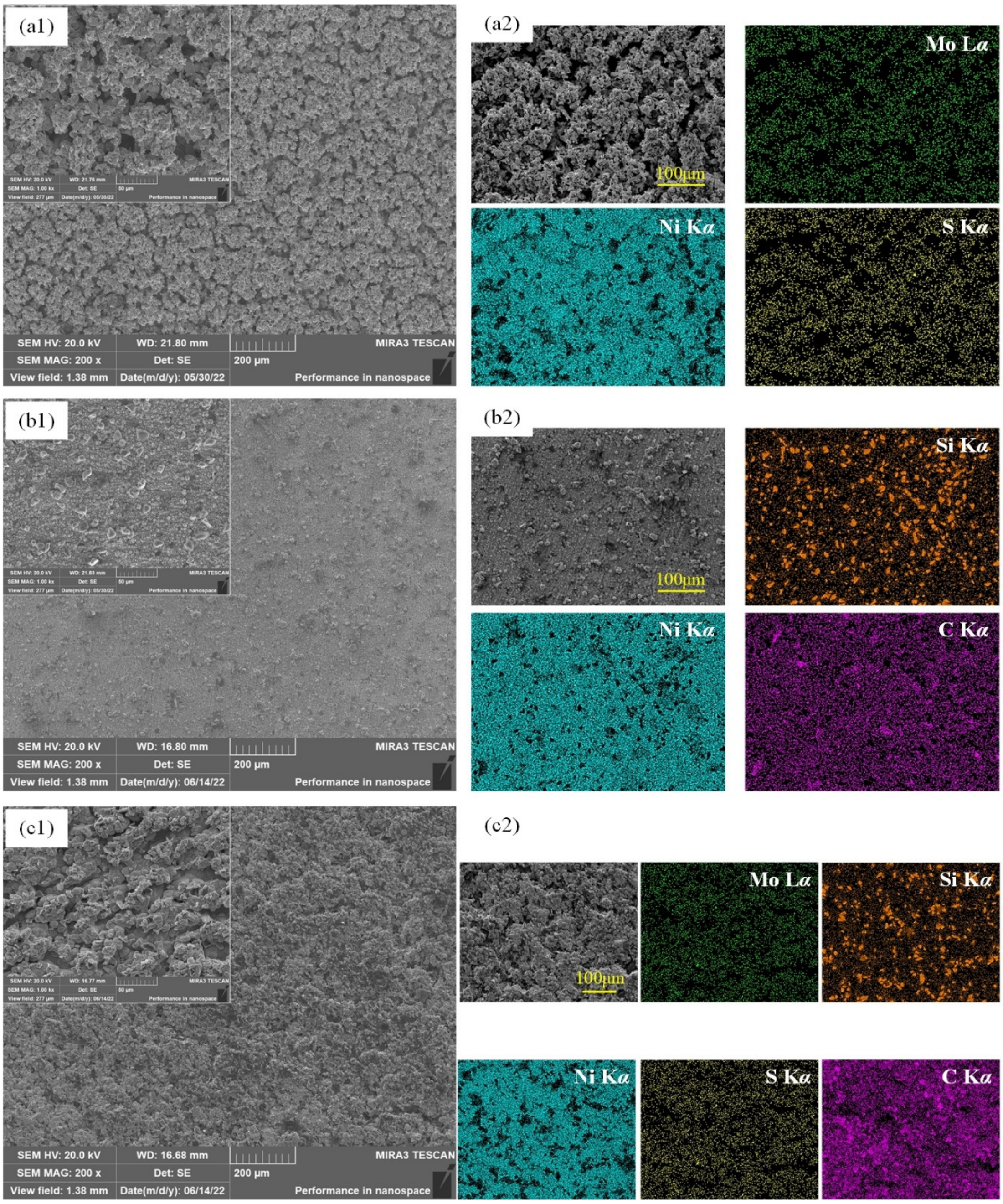

Figure 3. SEM images and EDS mappings for composite coating samples. (**a1**,**a2**) E1 sample; (**b1**,**b2**) E2 sample; (**c1**,**c2**) E3 sample.

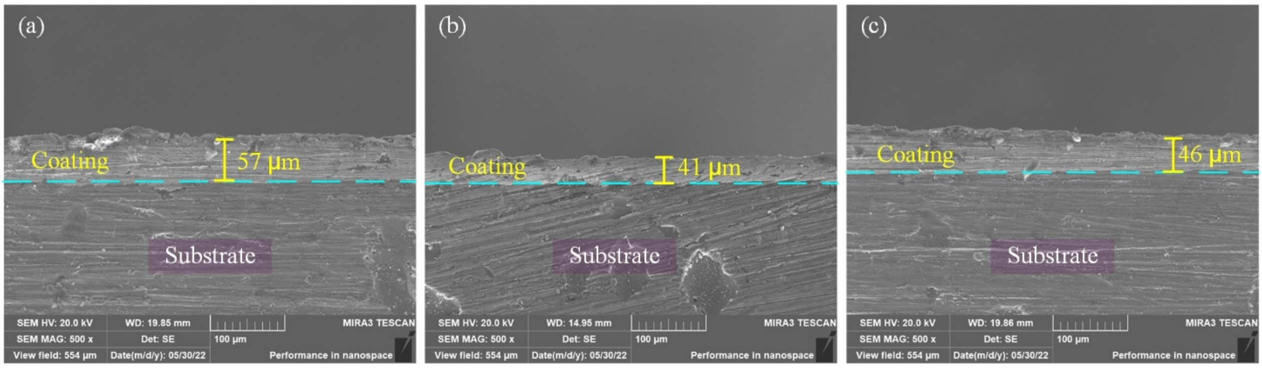

Figure 4. SEM images for the cross-section. (**a**) E1 sample; (**b**) E2 sample; (**c**) E3 sample.

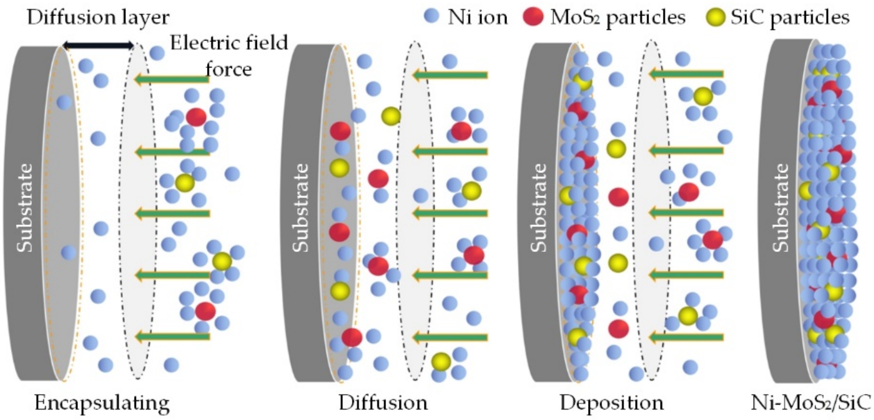

Figure 5. A schematic illustration of electrodeposition process.

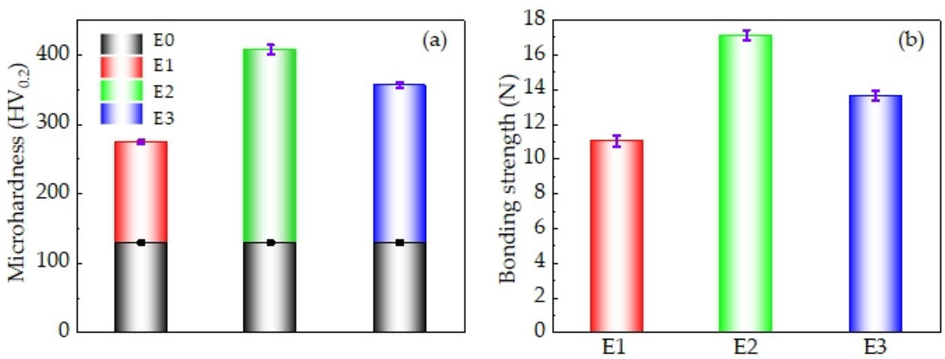

Figure 6. Mechanical properties of E0, E1, E2 and E3 samples. (**a**) Microhardness; (**b**) bonding strength.

The bonding strength between the composite coating and the substrate plays a key role in improving the tribological performances of a material by means of coating techniques [51,52]. The evaluation method for determining the bonding strength using a critical normal load is reported in references [41,53]. In this case, the critical normal load of each composite coating is obtained by the scratching method based on the measurement of friction and acoustic signals. During the test, the acoustic signal exhibits a stable low value when the diamond pin is just touching the composite coating. However, the acoustic signal will fluctuate and increase sharply when the severe plastic deformation and peeling off occurs. At this time, it indicates that the diamond pin has contacted the substrate [52]. As shown in Figure 6b, the measured critical normal loads of the E1, E2 and E3 samples are 11.03, 17.13 and 13.67 N, respectively. It can be found that the bonding strength of the E2 sample is the best, which is 55.30% and 25.31% higher than that of the E1 and E3 samples, respectively. It implies that the wear resistance of the E2 sample is superior to other composite coatings. It can be inferred that the interfacial bonding strength depends mainly on the pretreatment of the substrate surface, the characteristics of the coating materials and the electrodeposition conditions.

3.3. Tribological Performances

Figure 7 illustrates the variation characteristics of the wear rate and friction coefficient of the E0, E1, E2 and E3 samples. As shown in Figure 7a, it can be found that the wear rates of the composite coating samples are all much lower than that of the E0 sample, which indicates that the composite coatings enhance the wear resistance of the 2218 aluminum alloy substrate. The E0 sample has the maximal wear rate of 7.03 mg/N·m, indicating its poor wear resistance. The wear rate of the E2 sample is the minimum, which is 39.83% of the E0 sample. Compared with the E0 sample, the wear rates of the E1 and E3 samples are decreased by 28.88% and 43.10%, respectively. Therefore, it can be concluded that the wear resistance of the E3 sample is inferior to the E2 sample but better than the E1 sample. It can be clearly observed that the friction coefficient rapidly increases at the beginning of the test, and then increases slowly and finally fluctuates in a stable interval. Nevertheless, the friction response time is different for each sample, as illustrated in Figure 7b. The response times of the E1, E2 and E3 samples are significantly lower than that of the E0 sample. The E0 sample takes approximately 410 s to reach a stable friction state. However, the response time of the E1 sample is about 60 s, which is only 14.63% of the E0 sample. The response times and variation patterns of the E2 and E3 samples are essentially the same. For tribological problems, the rapid achievement of a stable friction state can effectively improve its working performances and reduce friction energy consumption. As shown in Figure 7c, it can be found that the average friction coefficient of all composite coating samples is significantly lower than that of the 2218 aluminum alloy substrate. The average friction coefficient of the E0 sample is 0.665, indicating its poor friction reduction. Compared with the E0 sample, the average friction coefficients of the E1, E2 and E3 samples are decreased by 59.70%, 33.98% and 52.63%, respectively. Therefore, the friction reduction of the E1 sample is the best. However, it is worth noting that the average friction coefficient of the E3 sample is increased by 14.92% compared to the E1 sample, while it is decreased by 48.57% compared to the E2 sample.

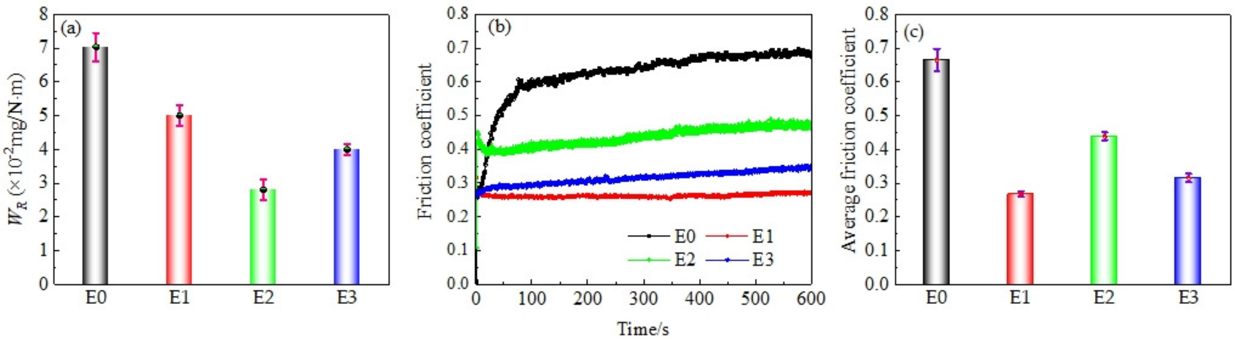

Figure 7. Variation of wear rate and friction coefficient of E0, E1, E2 and E3 samples. (**a**) Wear rate; (**b**) friction coefficient vs. time; (**c**) average friction coefficient.

Based on the above analysis, it can be found that all composite coating samples can effectively enhance the tribological behaviors of the 2218 aluminum alloy substrate, and the same results have been reported by other researchers [23,38,46,50]. Interestingly, the experimental results show that there are inconsistencies in the wear resistance and friction reduction of the same composite coating sample. For example, the wear resistance of the E2 sample is the best, while the friction reduction of the E1 sample is the best. For a practical engineering application, if there is a high demand for both friction reduction and wear resistance, a composite coating with comprehensive performance should be selected, such as the E3 sample in this paper. It is well known that the wear resistance of a material is proportional to its surface microhardness according to Archard's wear law [54–56]. Therefore, the enhancement of wear resistance of the composite coating should be mainly attributed to the improvement of the surface hardness. It can be concluded that the improved friction reduction of the composite coating containing MoS_2 is mainly attributed to its excellent lubricating properties and the formation of a good lubricating film between the friction interfaces by excited MoS_2 [25,30,57]. Meanwhile, the increased surface hardness of all composite coatings leads to a reduction in the adhesive wear, which also enhances its friction reduction properties.

The SEM images and 3D morphologies of worn surfaces of all samples are shown in Figure 8. It can be clearly observed that the worn surface exhibits obvious wide and deep grooves along the sliding direction, and there is typical plastic deformation and plastic flow, which is mainly due to the lower hardness of the 2218 aluminum alloy substrate. Likewise, a few microcracks and debris are present. The worn surface is much rougher, and the wear depth is 22.690 μm, as shown in Figure 8(a1,a2). The E0 sample exhibits typical severe adhesive wear and abrasive wear. However, the worn surface characteristics of all composite coatings are significantly different from that of the 2218 aluminum alloy substrate. As shown in Figure 8(b1,b2), the worn surface of the E1 sample is smoother and has the characteristics of smear wear, with very shallow and fine grooves distributed along the sliding direction. The wear depth is 5.230 μm, which is only 23.05% of the E0 sample. It can be assumed that the softer MoS_2 is released on the contact surface under the experimental conditions, forming a good lubricating layer and filling the grooves to some extent [57]. Considering the higher surface hardness of the E1 sample, this is the reason why this sample has very good friction reduction and wear resistance properties compared to the E0 sample, which corresponds to the results in Figure 7a,c. In the meantime, it can be observed that there are tiny pieces of debris, tearing and larger flake spalling on the worn surface, which are related to the characteristics of the composite coating. The mild abrasive wear, flake spalling and tearing are the main wear characteristics of the E1 sample. As shown in Figure 8(c1,c2), it can be observed that the worn surface of the E2 sample is relatively rough, with an obvious distribution of continuous relatively deep and wide grooves along the sliding direction. In addition, there are tiny pieces of debris, piled up debris and pits. The shedding of the SiC particles forms pits, and the plowing effect of the shedding SiC particles and hard debris on the worn surface cause the grooves to become deeper. However, the increase in surface hardness of the composite coating significantly reduced the depth of the grooves compared to the E0 sample. The results of Huang et al. [16] also reported similar wear characteristics of Ni-SiC composite coating. The wear depth of the E2 sample is 7.824 μm, which is 34.48% of that of the E0 sample and 1.50 times of that of the E1 sample. It can be concluded that the improved tribological behaviors of the E2 sample are mainly attributed to its increased surface microhardness. The E2 sample mainly exhibited abrasive wear and particle shedding. Compared with the E1 and E2 samples, the worn surface of the E3 sample is smooth and continuous, with relatively obvious distribution of continuous fine grooves along the sliding direction, smaller flakes spalling, pits caused by dislodged SiC particles and tearing of the composite coating. Nevertheless, there are no obvious plastic deformations and debris piled up. The wear depth of the E3 sample is 7.387 μm, which is 1.41 times that of the E1 sample and 94.41% that of the E2 sample. The good tribological properties of the composite coatings mainly depend on the improvement of their surface hardness and the combined friction reduction and wear resistance properties of the coating materials. However, the groove-filling ability of MoS_2 is diminished by the plowing effect of the hard particles. The tearing and flake spalling marks are significantly reduced. The E3 sample mainly exhibits mild abrasive wear, tearing and spalling, as shown in Figure 8(d1,d2). Therefore, when the friction reduction and wear resistance are considered together, the E3 sample has better tribological properties, which is consistent with the results of friction coefficient and wear rate in Figure 7.

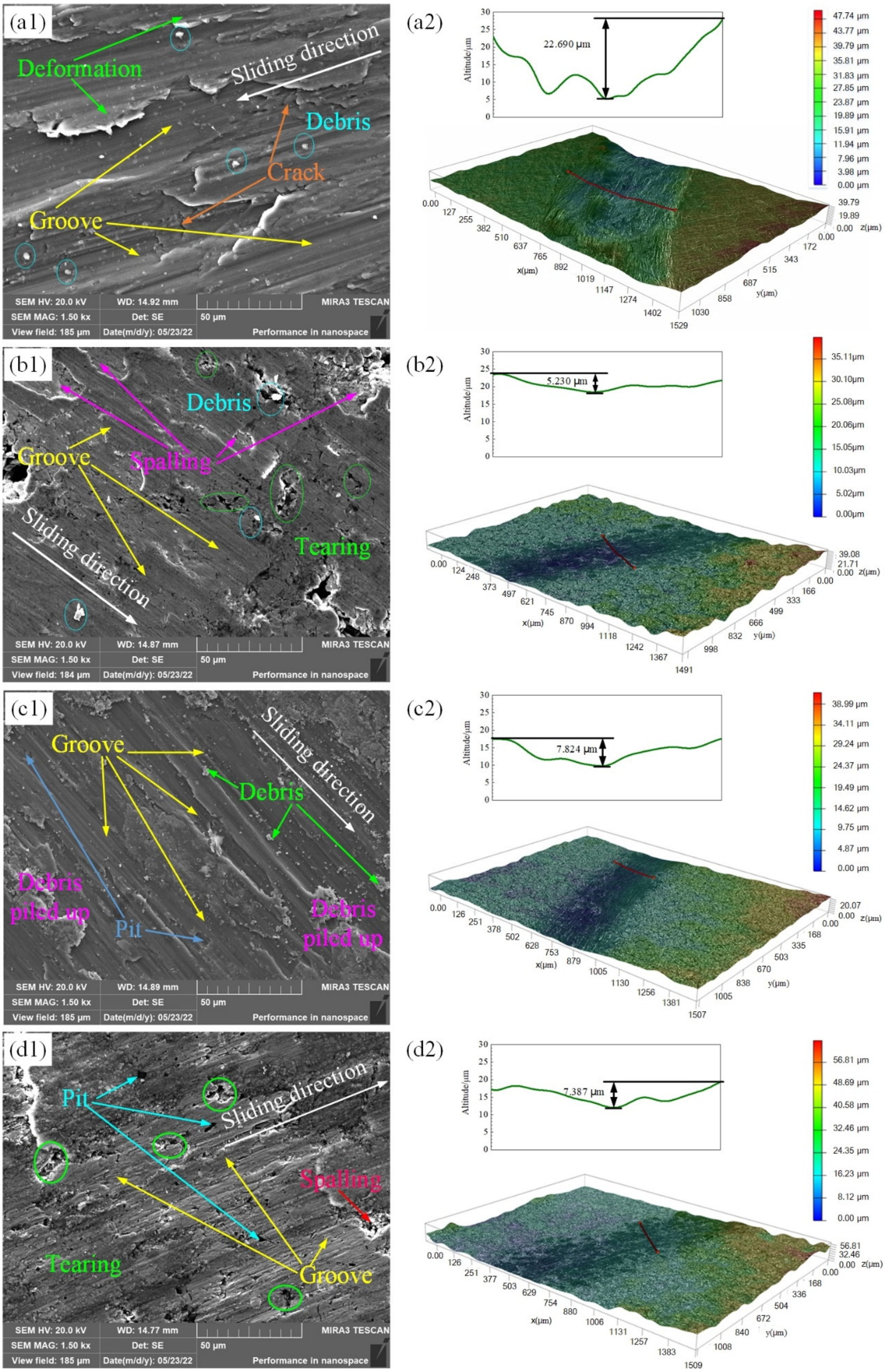

Figure 8. SEM images and 3D morphologies of the worn surface. (**a1**,**a2**) E0 sample; (**b1**,**b2**) E1 sample; (**c1**,**c2**) E2 sample; (**d1**,**d2**) E3 sample.

4. Conclusions

The Ni-MoS_2, Ni-SiC and Ni-MoS_2/SiC composite coatings were prepared by an electrodeposition method. The surface morphologies, microstructure, mechanical properties and tribological behaviors were investigated. The main conclusions are as follows:

(1) Compared with the 2218 aluminum alloy sample, the surfaces of the composite coating samples are rough. The coating materials are irregularly and relative uniformly distributed on the surface, the microstructure is compact, integral and consequent, tightly fitted with the substrate, without visible microcracks and pinhole defects. The thickness of the composite coating samples is different due to the different coating materials and their effects on the deposition rate.

(2) The surface microhardnesses of the Ni-MoS_2, Ni-SiC and Ni-MoS_2/SiC composite coating samples are 274.9 HV, 407.48 HV and 356.9 HV, which are 111.92%, 214.12% and 175.13% higher than that of the 2218 aluminum alloy substrate sample, respectively. It mainly depends on the strengthening effect of coating particles, grain refinement effect and fine microstructure.

(3) The tribological behaviors of all composite coating samples are significantly enhanced. The wear rates of Ni-MoS_2, Ni-SiC and Ni-MoS_2/SiC composite coating samples are 5 mg/N·m, 2.8 mg/N·m and 4 mg/N·m, and decreased by 28.87%, 60.17% and 43.10%, respectively. The average friction coefficients of corresponding samples are 0.2677, 0.4387 and 0.3153, and reduced by 59.73%, 34.01% and 52.56%, respectively. Therefore, the Ni-MoS_2/SiC composite coating sample is better from the viewpoint of comprehensive friction reduction and wear resistance.

(4) The predominant wear mechanism of the 2218 aluminum alloy substrate is severe adhesive wear and abrasive wear, which shows poor wear resistance.

(5) The Ni-MoS_2 composite coating sample is mainly characterized by mild abrasive wear, flake spalling and tearing. The Ni-SiC composite coating sample shows abrasive wear, particle shedding and piled up debris. However, the Ni-MoS_2/SiC composite coating sample exhibits typical mild abrasive wear, spalling, pits and tearing.

Author Contributions: Conceptualization, Y.Y. and Y.H.; methodology, Y.Y., L.L. and Y.H.; validation, Y.Y. and L.L.; formal analysis, Y.Y.; investigation, L.L., Y.Y. and Y.H.; resources, Y.Y. and Y.H.; data curation, Y.Y. and L.L.; writing—original draft preparation, Y.Y., L.L. and Y.Z.; writing—review and editing, Y.Y.; visualization, Y.Y. and L.L.; supervision, Y.Y. and Y.H.; project administration, Y.Y.; funding acquisition, Y.Y. All authors have read and agreed to the published version of the manuscript.

Funding: This research was funded by the National Natural Science Foundation of China, grant number 51875095.

Institutional Review Board Statement: Not applicable.

Informed Consent Statement: Not applicable.

Data Availability Statement: The data presented in this work are available on request from the corresponding authors.

Conflicts of Interest: The authors declare no conflict of interest.

References

1. Holmberg, K.; Kivikytö-Repo, P.; Härkisaari, P.; Valtonen, K.; Erdemir, A. Global energy consumption due to friction and wear in the mining industry. *Tribol. Int.* **2017**, *15*, 116–139. [CrossRef]
2. Li, J.; Qiu, H.; Zhang, X.F.; Yu, H.L.; Yang, J.J.; Tu, X.H.; Li, W. Effects of (Ti, Mo) C particles on the abrasive wear-corrosion of low alloy martensitic steel. *Wear* **2022**, *496–497*, 204288. [CrossRef]
3. Mahidashti, Z.; Aliofkhazraei, M.; Lotfi, N. Review of nickel-based electrodeposited tribo-coatings. *Trans. Indian Inst. Met.* **2018**, *71*, 257–295. [CrossRef]
4. Wang, J.Z.; Jiang, S.W.; Song, S.; Wang, Z.Q. Addition of molybdenum disulfide solid lubricant to WC-12Ni thermal spray cemented carbide powders through electroless Ni-MoS_2 co-deposition. *J. Alloys Compd.* **2019**, *786*, 594–606. [CrossRef]
5. Kosta, I.; García, I.; Chuvilin, A.; Medina, E.; Grande, H.; Tena-Zaera, R. Ionic liquid-based electrodeposition of ZnS: Nano-MoS_2 composite films with self-lubricating properties. *Surf. Coat. Technol.* **2019**, *374*, 957–965. [CrossRef]

6. Rajaei, H.; Menapace, C.; Straffelini, G.; Gialanella, S. Characterization, wear and emission properties of MnS containing laser cladded brake disc. *Wear* **2022**, *504*, 204405. [CrossRef]
7. Vasić, B.; Ralević, U.; Cvetanović Zobenica, K.; Smiljanić, M.M.; Gajić, R.; Spasenović, M.; Vollebregt, S. Low-friction, wear-resistant, and electrically homogeneous multilayer graphene grown by chemical vapor deposition on molybdenum. *Appl. Surf. Sci.* **2020**, *509*, 144792. [CrossRef]
8. Babur, M.Z.; Iqbal, Z.; Shafiq, M.; Naz, M.Y.; Makhlouf, M.M. Hybrid TiN-CCPN coating of AISI-201 stainless steel by physical vapor deposition combined with cathodic cage plasma nitriding for improved tribological properties. *J. Build. Eng.* **2022**, *45*, 103512. [CrossRef]
9. Testa, V.; Morelli, S.; Bolelli, G.; Lusvarghi, L.; Björklund, S.; Joshi, S. Micromechanical behaviour and wear resistance of hybrid plasma-sprayed TiC reinforced tribaloy-400. *Surf. Coat. Technol.* **2021**, *425*, 127682. [CrossRef]
10. Wang, H.; Liu, H.J.; He, Y.; Ma, C.Y.; Li, L.Z. Ni-SiC composite coatings with good wear and corrosion resistance synthesized via ultrasonic electrodeposition. *J. Mater. Eng. Perform.* **2021**, *30*, 1535–1544. [CrossRef]
11. Sivasakthi, P.; Sangaranarayanan, M.V. Influence of pulse and direct current on electrodeposition of Ni-Gd_2O_3 nanocomposite for micro hardness, wear resistance and corrosion resistance applications. *Compos. Commun.* **2019**, *13*, 134–142. [CrossRef]
12. Tamilarasan, T.R.; Sanjith, U.; Rajendran, R.; Rajagopal, G.; Sudagar, J. Effect of reduced graphene oxide reinforcement on the wear characteristics of electroless Ni-P coatings. *J. Mater. Eng. Perform.* **2018**, *27*, 3044–3053. [CrossRef]
13. Krajaisri, P.; Puranasiri, R.; Chiyasak, P.; Rodchanarowan, A. Investigation of pulse current densities and temperatures on electrodeposition of tin-copper alloys. *Surf. Coat. Technol.* **2022**, *435*, 128244. [CrossRef]
14. Fuseini, M.; Zaghloul, M.M.Y. Investigation of electrophoretic deposition of PANI nano fibers as a manufacturing technology for corrosion protection. *Prog. Org. Coat.* **2022**, *171*, 107015. [CrossRef]
15. Fuseini, M.; Zaghloul, M.M.Y. Statistical and qualitative analyses of the kinetic models using electrophoretic deposition of polyaniline. *J. Ind. Eng. Chem.* **2022**, *113*, 475–487. [CrossRef]
16. Huang, P.C.; Hou, K.H.; Hong, J.J.; Lin, M.H.; Wang, G.L. Study of fabrication and wear properties of Ni-SiC composite coatings on A356 aluminum alloy. *Wear* **2021**, *477*, 203772. [CrossRef]
17. Fathi, M.; Safavi, M.S.; Mahdavi, S.; Mirzazadeh, S.; Charkhesht, V.; Mardanifar, A.; Mehdipour, M. Co-P alloy matrix composite deposits reinforced by nano-MoS_2 solid lubricant: An alternative tribological coating to hard chromium coatings. *Tribol. Int.* **2021**, *159*, 106956. [CrossRef]
18. Singh, S.; Samanta, S.; Das, A.K.; Sahoo, R.R. Hydrophobic reduced graphene oxide-based Ni coating for improved tribological application. *J. Mater. Eng. Perform.* **2019**, *28*, 3704–3713. [CrossRef]
19. Liu, J.S.; Shi, Y. Microstructure and wear behavior of laser-cladded Ni-based coatings decorated by graphite particles. *Surf. Coat. Technol.* **2021**, *412*, 127044. [CrossRef]
20. Parthiban, K.; Lakshmanan, P.; Palani, S.; Arumugam, A. Electroless deposition of SiC Nano coating on aluminium alloy and evaluation of wear resistance and electroless characteristics. *Mater. Today Proc.* **2021**, *46*, 1096–1100. [CrossRef]
21. Zhou, Y.; Sun, Z.P.; Yu, Y.; Li, L.; Song, J.L.; Xie, F.Q.; Wu, X.Q. Tribological behavior of Ni-SiC composite coatings produced by circulating-solution electrodeposition technique. *Tribol. Int.* **2021**, *159*, 106933. [CrossRef]
22. Sun, C.F.; Liu, X.Q.; Zhou, C.Y.; Wang, C.N.; Cao, H.W. Preparation and wear properties of magnetic assisted pulse electrodeposited Ni-SiC nanocoatings. *Ceram. Int.* **2019**, *45*, 1348–1355. [CrossRef]
23. Yazdani, A.; Zakeri, A. Fabrication and characterization of Ni-SiC nanocomposite coatings on Al substrates by ball impact deposition method. *Metall. Mater. Trans. A* **2017**, *48*, 4180–4192. [CrossRef]
24. Ji, R.J.; Han, K.; Jin, H.; Li, X.P.; Liu, Y.H.; Liu, S.G.; Dong, T.C.; Cai, B.P.; Cheng, W.H. Preparation of Ni-SiC nano-composite coating by rotating magnetic field-assisted electrodeposition. *J. Manuf. Process.* **2020**, *57*, 787–797. [CrossRef]
25. Pinate, S.; Leisner, P.; Zanella, C. Wear resistance and self-lubrication of electrodeposited Ni-SiC: MoS_2 mixed particles composite coatings. *Surf. Coat. Technol.* **2021**, *421*, 127400. [CrossRef]
26. Wu, Y.T.; Liu, L.; Shen, B.; Hu, W.B. Study of self-lubricant Ni-P-PTFE-SiC composite coating. *J. Mater. Sci.* **2005**, *40*, 5057–5059. [CrossRef]
27. Harshavardhan, K.; Nagendran, S.; Shanmugasundaram, A.; Pravin Sankar, S.R.; Sai Kowshik, K. Investigating the effect of reinforcing SiC and graphite on aluminium alloy brake rotor using plasma spray process. *Mater. Today Proc.* **2021**, *38*, 2706–2712. [CrossRef]
28. Gyawali, G.; Kim, H.S.; Tripathi, K.; Kim, T.H.; Lee, S.W. Fabrication and characterization of electrodeposited Ni-SiC-h/BN composite coatings. *J. Mater. Sci. Technol.* **2014**, *30*, 796–802. [CrossRef]
29. Khodaei, M.; Gholizadeh, A.M. SiC nanoparticles incorporation in electroless NiP-graphene oxide nanocomposite coatings. *Ceram. Int.* **2021**, *47*, 25287–25295. [CrossRef]
30. Maharana, H.S.; Mondal, K. Manifestation of Hall-Petch breakdown in nanocrystalline electrodeposited Ni-MoS_2 coating and its structure dependent wear resistance behavior. *Surf. Coat. Technol.* **2021**, *410*, 126950. [CrossRef]
31. He, Y.; Wang, S.C.; Walsh, F.C.; Chiu, Y.L.; Reed, P.A.S. Self-lubricating Ni-P-MoS_2 composite coatings. *Surf. Coat. Technol.* **2016**, *307*, 926–934. [CrossRef]
32. Wang, P.; Yue, W.; Lu, Z.B.; Zhang, G.G.; Zhu, L.N. Friction and wear properties of MoS_2-based coatings sliding against Cu and Al under electric current. *Tribol. Int.* **2018**, *127*, 379–388. [CrossRef]

33. Krauß, S.; Seynstahl, A.; Tremmel, S.; Meyer, B.; Bitzek, E.; Göoken, M.; Yokosawa, T.; Zubiri, B.A.; Spiecker, E.; Merle, B. Structural reorientation and compaction of porous MoS_2 coatings during wear testing. *Wear* **2022**, *500–501*, 204339. [CrossRef]
34. Serles, P.; Sun, H.; Colas, G.; Tam, J.; Nicholson, E.; Wang, G.R.; Howe, J.; Saulot, A.; Singh, C.V.; Filleter, T. Structure-dependent wear and shear mechanics of nanostructured MoS_2 coatings. *Adv. Mater. Interfaces* **2020**, *7*, 1901870. [CrossRef]
35. Hou, K.M.; Yang, S.R.; Liu, X.H.; Wang, J.Q. The self-ordered lamellar texture of MoS_2 transfer film formed in complex lubrication. *Adv. Mater. Interfaces* **2018**, *5*, 1701682. [CrossRef]
36. Vierneusel, B.; Schneider, T.; Tremmel, S.; Wartzack, S.; Gradt, T. Humidity resistant MoS_2 coatings deposited by unbalanced magnetron sputtering. *Surf. Coat. Technol.* **2013**, *235*, 97–107. [CrossRef]
37. Zhang, J.W.; Wang, Y.X.; Zhou, S.G.; Wang, Y.C.; Wang, C.Y.; Guo, W.M.; Lu, X.J.; Wang, L.P. Tailoring self-lubricating, wear-resistance, anticorrosion and antifouling properties of Ti/(Cu, MoS_2)-DLC coating in marine environment by controlling the content of Cu dopant. *Tribol. Int.* **2020**, *143*, 106029. [CrossRef]
38. Lin, Q.L.; Wang, X.; Cai, M.; Yan, H.; Zhao, Z.; Fan, X.Q.; Zhu, M.H. Enhancement of Si_3N_4@MoS_2 core–shell structure on wear/corrosion resistance of epoxy resin/polyacrylate IPN composite coating. *Appl. Surf. Sci.* **2021**, *568*, 150938. [CrossRef]
39. Maji, P.; Nath, R.K.; Paul, P.; Bhogendro Meitei, R.K.; Ghosh, S.K. Effect of processing speed on wear and corrosion behavior of novel MoS_2 and CeO_2 reinforced hybrid aluminum matrix composites fabricated by friction stir processing. *J. Manuf. Process.* **2021**, *69*, 1–11. [CrossRef]
40. Pancrecious, J.K.; Deepa, J.P.; Jayan, V.; Bill, U.S.; Rajan, T.P.D.; Pai, B.C. Nanoceria induced grain refinement in electroless Ni-B-CeO_2 composite coating for enhanced wear and corrosion resistance of aluminium alloy. *Surf. Coat. Technol.* **2018**, *356*, 29–37. [CrossRef]
41. Chen, W.L.; Zheng, J.; Lin, Y.; Kwon, S.; Zhang, S.H. Comparison of AlCrN and AlCrTiSiN coatings deposited on the surface of plasma nitrocarburized high carbon steels. *Appl. Surf. Sci.* **2015**, *332*, 525–532. [CrossRef]
42. Jia, D.L.; Yi, P.; Liu, Y.C.; Jia, H.Y.; Yang, X.S. Effect of the width and depth of laser-textured grooves on the bonding strength of plasma-sprayed coatings in the scratch direction. *Mater. Sci. Eng. A* **2021**, *820*, 141558. [CrossRef]
43. Shourije, S.M.J.S.; Bahrololoom, M.E. Effect of current density, MoS_2 content and bath agitation on tribological properties of electrodeposited nanostructured NiMoS2 composite coatings. *Tribol.-Materals Surf. Interfaces* **2019**, *13*, 76–87. [CrossRef]
44. Zhou, N.; Wang, S.C.; Walsh, F.C. Effective particle dispersion via high-shear mixing of the electrolyte for electroplating a nickel-molybdenum disulphide composite. *Electrochim. Acta* **2018**, *283*, 568–577. [CrossRef]
45. Gyawali, G.; Cho, S.H.; Woo, D.J.; Lee, S.W. Pulse electrodeposition and characterisation of Ni-SiC composite coatings in presence of ultrasound. *Trans. Inst. Met. Finish.* **2012**, *90*, 274–281. [CrossRef]
46. Gyawali, G.; Joshi, B.; Tripathi, K.; Lee, S.W. Effect of Ultrasonic nanocrystal surface modification on properties of electrodeposited Ni and Ni-SiC composite coatings. *J. Mater. Eng. Perform.* **2017**, *26*, 4462–4469. [CrossRef]
47. Uysal, M. Electroless codeposition of Ni-P composite coatings: Effects of graphene and TiO_2 on the morphology, corrosion, and tribological properties. *Metall. Mater. Trans. A* **2019**, *50*, 2331–2341. [CrossRef]
48. Yan, Y.T.; Jiang, C.; Huo, Y.Q.; Li, C.F. Preparation and tribological behaviors of lubrication-enhanced PEEK composites. *Appl. Sci.* **2020**, *10*, 7536. [CrossRef]
49. Yang, C.; Zhu, J.Y.; Cui, S.H.; Chen, P.H.; Wu, Z.C.; Ma, Z.Y.; Fu, R.K.Y.; Tian, X.B.; Chu, P.K.; Wu, Z.Z. Wear and corrosion resistant coatings prepared on LY12 aluminum alloy by plasma electrolytic oxidation. *Surf. Coat. Technol.* **2021**, *409*, 126885. [CrossRef]
50. Qiu, T.X.; Pan, S.Y.; Fan, C.; Zhu, X.F.; Shen, X.P. Effect of Ni-coated MoS_2 on microstructure and tribological properties of (Cu-10Sn)-based composites. *Trans. Nonferrous Met. Soc. China* **2020**, *30*, 2480–2490. [CrossRef]
51. Wang, L.; Liu, S.Y.; Gou, J.F.; Zhang, Q.W.; Zhou, F.F.; Wang, Y.; Chu, R.Q. Study on the wear resistance of graphene modified nanostructured Al_2O_3/TiO_2 coatings. *Appl. Surf. Sci.* **2019**, *492*, 272–279. [CrossRef]
52. Dong, B.Z.; Guo, X.H.; Zhang, K.D.; Zhang, Y.P.; Li, Z.B.; Wang, W.S.; Cai, C. Combined effect of laser texturing and carburizing on the bonding strength of DLC coatings deposited on medical titanium alloy. *Surf. Coat. Technol.* **2022**, *429*, 127951. [CrossRef]
53. Li, W.Y.; Yang, X.F.; Wang, S.R.; Duan, D.R.; Li, F.J.; Qiao, Y.; Liu, Y.L.; Liu, X.P. The effect of WC content on the bonding strength and mechanical properties of WC/Ni60 coatings of brake disc. *Opt. Laser Technol.* **2022**, *149*, 107822. [CrossRef]
54. Wang, J.L.; Su, Y.; Alagu Subramaniam, N.; Pang, J.H.L. Archard model guided feature engineering improved support vector regression for rail wear analysis. *Eng. Fail. Anal.* **2022**, *137*, 106248. [CrossRef]
55. Reichelt, M.; Cappella, B. Large scale multi-parameter analysis of wear of self-mated 100Cr6 steel-A study of the validity of Archard's law. *Tribol. Int.* **2021**, *159*, 106945. [CrossRef]
56. Yan, Y.T.; Jiang, C.; Li, W.D. Simulation on coupling effects between surface wear and fatigue in spur gear. *Eng. Fail. Anal.* **2022**, *134*, 106055. [CrossRef]
57. Furlan, K.P.; de Mello, J.D.B.; Klein, A.N. Self-lubricating composites containing MoS_2: A review. *Tribol. Int.* **2018**, *120*, 280–298. [CrossRef]